29. T. Tanaka, *Phys. Rev. Lett.* **40**, 820 (1978).
30. We thank G. Cohen for help in writing this manuscript. This work was supported by Israel Science Foundation Bikura program (no. 1437/04), German-Israeli Foundation, United States–Israel Binational Foundation (grant no. 2004037), and the MechPlant project of European Union's New and Emerging Science and Technology program.

Supporting Online Material
www.sciencemag.org/cgi/content/full/315/5815/1116/DC1
Materials and Methods
Fig. S1
Movie S1

6 October 2006; accepted 18 January 2007
10.1126/science.1135994

Focusing Beyond the Diffraction Limit with Far-Field Time Reversal

Geoffroy Lerosey, Julien de Rosny, Arnaud Tourin, Mathias Fink*

We present an approach for subwavelength focusing of microwaves using both a time-reversal mirror placed in the far field and a random distribution of scatterers placed in the near field of the focusing point. The far-field time-reversal mirror is used to build the time-reversed wave field, which interacts with the random medium to regenerate not only the propagating waves but also the evanescent waves required to refocus below the diffraction limit. Focal spots as small as one-thirtieth of a wavelength are described. We present one example of an application to telecommunications, which shows enhancement of the information transmission rate by a factor of 3.

Subwavelength information about an object is carried by evanescent waves. As they decay exponentially, these evanescent waves are generally lost before reaching the far-field image plane, which is the origin of the diffraction limit. One approach to recover evanescent waves in near-field microscopy is to place a subwavelength scatterer in the near field of the object to be imaged. By diffracting off the scatterer, evanescent waves can convert into propagating waves, which can then be detected in the far field. In the past decade, several schemes for detecting evanescent waves were introduced (*1*, *2*). They use either a subwavelength-sized aperture or a sharp stylus that samples the field very close (<λ) to the specimen to be imaged.

More recently, superlenses have been proposed for imaging beyond the diffraction limit (*3*–*5*). These discoveries followed the original descriptions of negative refraction and perfect imaging of quasistatic line sources (*6*, *7*). Such superlenses consist of thin slabs of materials with negative permittivity, permeability, or both (*4*, *5*, *8*–*11*). Recently a cylindrical lens relying on anisotropic metamaterials has also been theoretically proposed (*12*). Superlenses transmit evanescent waves with enhanced amplitude, in contrast to conventional materials. Thus, evanescent components radiated by an object can be recovered in the image plane. In contrast with near-field microscopy, which requires a point-by-point scanning, superlenses form the whole image at once. One drawback is that in all existing experimental verifications, the image still forms in the near-field zone of the superlens and a scanning near-field microscopy technique must be used to create the far-field image (*13*).

Our approach for subwavelength focusing uses a focusing aperture placed in the far field. The idea is to build a microstructured medium in the near field of the point where one intends to focus and to use a time-reversal mirror (TRM) placed in the far field to build the time-reversed wave field that will focus at the target without being subject to the diffraction limit.

The time-reversal technique is well known in acoustics and has led to a number of applications in ultrasound and underwater acoustics, such as brain therapy, lithotripsy, and nondestructive testing, as well as in telecommunications (*14*). In a typical time-reversal experiment, an acoustic source is placed at the location where one intends to focus. First, this source sends out a short pulse. The wave field propagates and is recorded with a set of transducers located on a surface. Second, the recorded signals are flipped in time. Third, the flipped signals are transmitted back by the same set of transducers acting as transmitters. The resulting wave is found to converge back to its initial source. At best, if the transducers are located on a closed surface surrounding the original source, forming a closed TRM, the time-reversed wave converges from all directions. However, even if the original source is pointlike, the focal spot is not. Indeed, as the amplitude of the evanescent waves decays

Laboratoire Ondes et Acoustique, École Supérieure de Physique et de Chimie Industrielles, Université Paris VII, Centre National de la Recherche Scientifique, UMR 7587, 10 rue Vauquelin, 75005 Paris, France.

*To whom correspondence should be addressed. E-mail: mathias.fink@espci.fr

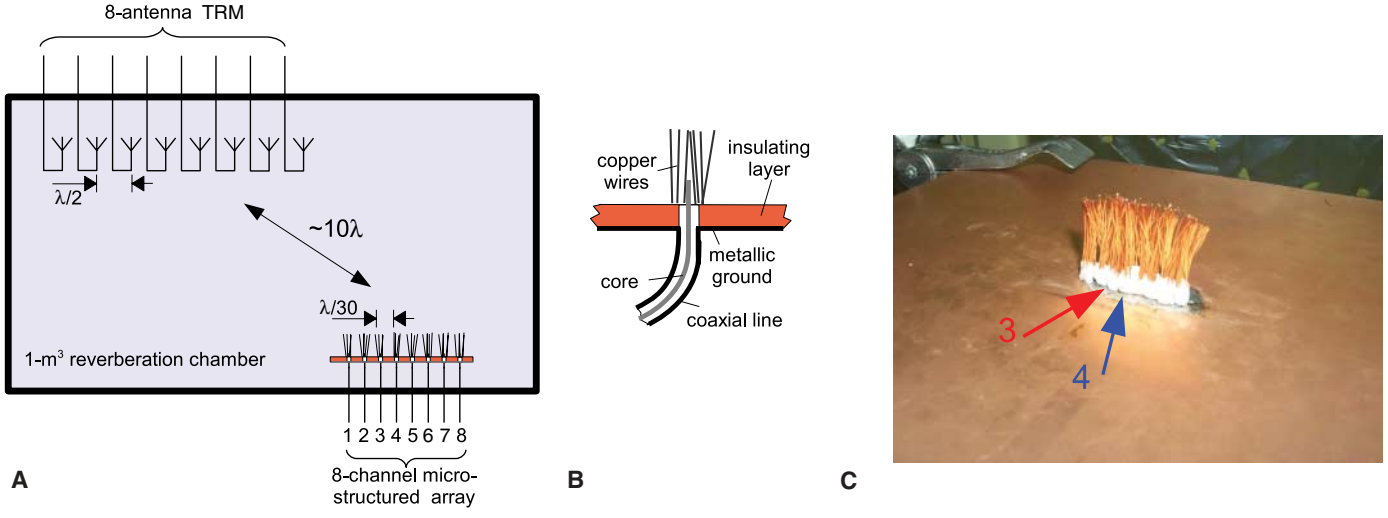

Fig. 1. Experimental setup. (**A**) A TRM made of eight commercial dipolar antennas operating at 2.45 GHz (i.e., λ = 12 cm) is placed in a 1-m^3 reverberating chamber. Ten wavelengths away from the TRM is placed a subwavelength receiving array consisting of eight microstructured antennas λ/30 apart from one another. (**B**) Details of one microstructured antenna. It consists of the core of a coaxial line that comes out 2 mm from an insulating layer and is surrounded by a microstructure consisting of a random distribution of thin copper wires. (**C**) Photo of the eight-element subwavelength array surrounded by the random distribution of copper wires. Antennas 3 and 4 are indicated by the red and blue arrows.

Downloaded from https://www.science.org at Indian Institute of Technology, Delhi on January 30, 2025

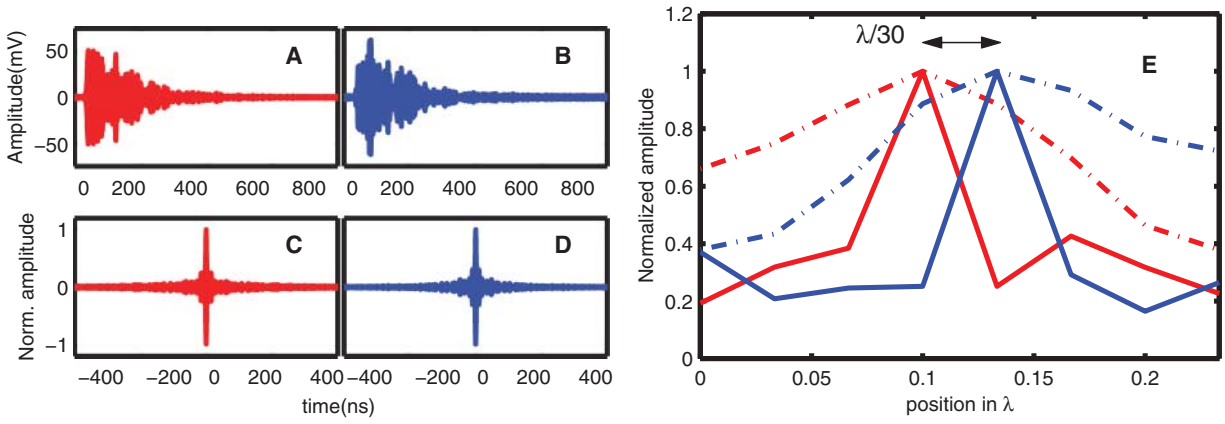

Fig. 2. Focusing beyond the diffraction limit. (**A** and **B**) show the signal received at one antenna of the TRM when a 10-ns pulse is sent from antennas 3 and 4, respectively, of the microstructured array. The signals in (A) and (B) look considerably different, although antennas 3 and 4 are only λ/30 apart. (**C** and **D**) show the time compression obtained at antennas 3 and 4, respectively, when the eight signals coming from antennas 3 and 4 are time-reversed and sent back from the TRM. (**E**) In full line are shown the focusing spots obtained around antennas 3 and 4. Their typical width is λ/30. Thus, antennas 3 and 4 can be addressed independently. The focal spots obtained when there are no copper wires are shown for comparison (dashed-dotted line). All maxima have been normalized by scaling factors in the ratios: 1 (red and blue dashed-dotted lines), 2.2 (red full line), 2.5 (blue full line).

exponentially, a closed TRM located in the far field cannot sense and retransmit the evanescent components. Therefore, the time-reversed field produces a λ/2 focal spot in agreement with the diffraction limit.

In practice, a closed TRM is difficult to realize. The time-reversal operation is usually performed on a limited angular area, but if the time-reversal experiment is conducted inside a reverberant chamber, the diffraction limit can actually be reached, even with a small-aperture TRM (*15*). In this case, the time-reversed wave focuses from all directions because of reverberation off boundaries. Recently, experimental demonstrations of phase conjugation and broadband time reversal were reported for microwaves (*16*–*18*). In our microwave time-reversal experiments, a TRM made of eight antennas operating at a central frequency of 2.45 GHz with a bandwidth of 150 MHz was able to focus on a λ/2 focal spot inside a reverberant chamber.

Our approach to recover evanescent waves is to place a random distribution of subwavelength scatterers in the near field of the source. By diffracting off the scatterers, evanescent waves can convert into propagating waves, which can then be detected by the far-field time-reversal mirror. These propagating waves are time-reversed in the far field and transmitted back. Because of the theorem of generalized reciprocity between evanescent waves and propagating waves (*19*), the part of the far-field time-reversed wave originating from the evanescent waves of the source is converted back into the initial evanescent components, which thus participate in the refocusing process. In contrast to superlenses, evanescent waves are not enhanced here but, as a result of reciprocity, are recovered in the back-propagation step of the time-reversal process.

We have applied this idea to microwaves. A source consists of a wire antenna operating at a central frequency of 2.45 GHz (i.e., λ = 12 cm).

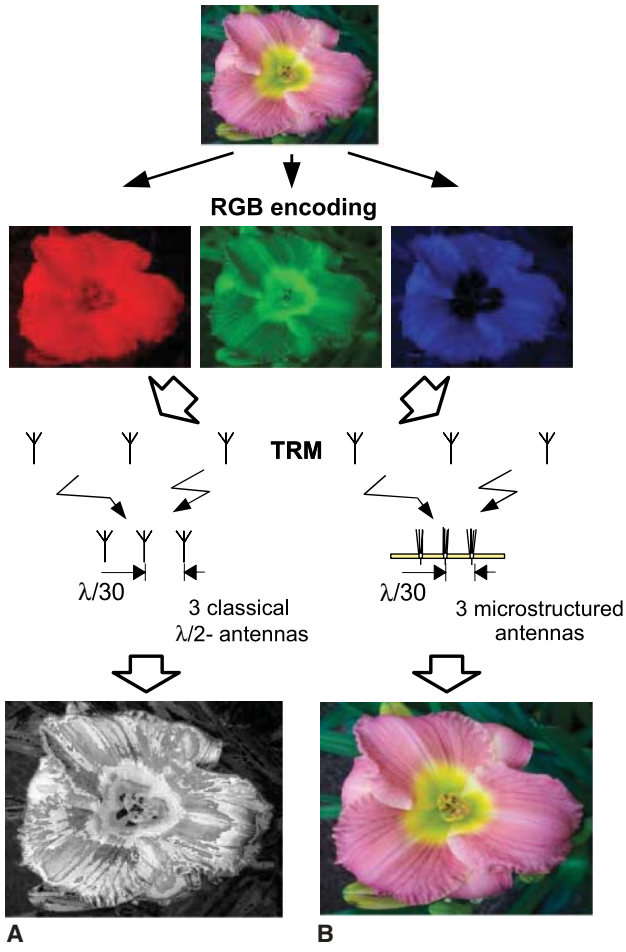

Fig. 3. Transmission of a color image. Transmission of a color image between a three-antenna TRM and a three-antenna receiving array. The original image is encoded on three RGB channels, and the three corresponding bitstreams are sent from the three antennas of the TRM. With a classical receiving array, the image is gray after decoding (**A**) because the three antennas coding for the red, green, and blue channels receive the same signal. With a microstructured receiving array, the red, green, and blue signals are focused independently on the three receiving antennas, although these latter are λ/30 apart from each other. The relative weights between the RGB channels are thus preserved and the color image is restored (**B**).

To convert the evanescent waves into propagating waves, the antenna is surrounded by a microstructure consisting of a random distribution of thin copper wires located in the near field of the antenna (see details of one antenna in Fig. 1, B and C). In our experiment, we consider eight possible focusing points placed in a strongly reverberating chamber (Fig. 1A). Eight microwave sources surrounded by a random microstructure are placed at these eight locations so that they can be used in the initial step of the time-reversal process. The distance between two adjacent antennas is λ/30. These eight antennas form an array that will be referred to as the re-

Downloaded from https://www.science.org at Indian Institute of Technology, Delhi on January 30, 2025

ceiving array. A TRM made of eight commercial dipolar antennas is placed in the far field, 10 wavelengths away from the receiving array. (The electronic part of the setup is described in fig. S1.) When antenna 3 sends a short pulse (10 ns), the eight signals received at the TRM are much longer than the initial pulse because of strong reverberation in the chamber (typically 500 ns). An example of the signal received at one of the antennas of the TRM is shown in Fig. 2A. When antenna 4 is used as a source, the signal received at the same antenna in the TRM (shown in Fig. 2B) is considerably different, although sources 3 and 4 are $\lambda/30$ apart. When these signals are time-reversed and transmitted back, the resulting waves converge respectively to antennas 3 and 4, where they recreate pulses as short as the initial ones (Fig. 2, C and D). Measuring the signal received at the other antennas of the receiving array gives access to the spatial focusing around antennas 3 and 4 (Fig. 2E). The two antennas can now be addressed independently, because the focusing spots created around them are much smaller than the wavelength (typically $\lambda/30$). The diffraction limit is overcome, although the focusing points are in the far field of the TRM.

The origin of the diffraction limit, and the way to overcome it, can be revisited by using the time-reversal concept and the Green's function formalism, without the explicit use of the evanescent wave concept (*20*–*22*). The time-reversed wave, generated by a closed TRM, which converges to its source, is always followed by a spatially diverging wave due to energy flux conservation. Because the focal spot results from the interference of these two waves, the time-reversed field can always be expressed (for a monochromatic wave) as the imaginary part of the Green's function (*22*). In a homogeneous medium, the imaginary part of the Green's function oscillates typically on a wavelength scale. To create focal spots much smaller than the wavelength, one introduces subwavelength scatterers in the near field of the source. Therefore, the spatial dependence of the imaginary part of the Green's function is modified to oscillate on scales much smaller than the wavelength.

A promising application of time-reversal subwavelength focusing is telecommunications. One way that has been proposed to increase the data rate of a communication system is to use multiantenna arrays at both transmitter and receiver (*23*); different bitstreams sent from each antenna of the transmitting array can be decoded at the receiving array under the condition that the medium creates sufficient scattering. It is also generally stated that the spacing between the receiving antennas must be larger than $\lambda/2$ (*23*). If these two conditions are fulfilled, the global maximum error-free data rate, or "Shannon Capacity," is at best multiplied by the number of transmitting antennas. Such methods are referred to as MIMO (multiple input–multiple output). However, from a practical perspective, it is difficult to ensure that the distance between antennas can be made large enough for this requirement to be satisfied. This difficulty is typically encountered when antennas are placed in a laptop and the telecommunication wavelengths are on the centimeter scale (e.g., Bluetooth or Wi-Fi). An illustration of the benefit of time-reversal subwavelength focusing to overcome this difficulty is given in Fig. 3. A three-antenna TRM is used to transmit a color picture to a three-antenna receiving array. The original picture is encoded onto three RGB (red-green-blue) color channels. Each corresponding figure is represented by a bit series giving the gray levels of each pixel on that particular channel. Then the simplest modulation is used (a positive pulse for bit 1, a negative one for bit 0) to create three bitstreams with a data rate of 50 Mbit/s each. The intended global data rate is thus 150 Mbit/s. Time reversal is used to focus each bitstream onto one of the antennas (one antenna for each color) of the receiving array. Then the three bitstreams are decoded and mixed to reconstruct the color image. The communication is performed with two kinds of receiving arrays. The first is "classical"; it consists of three dipolar antennas with a $\lambda/30$ spacing. The second is a microstructured antenna array analogous to the one previously described (Fig. 1). It turns out that the image reconstructed with the classical array is gray-scaled: Its colors are lost. Indeed, subwavelength spaced antennas are strongly coupled, that is, they essentially receive the same signal. Hence, each transmitted pixel is gray because the three different antennas corresponding to the three different color channels receive the same gray levels. However, when the microstructured receiving array is used, each color stream focuses independently at each antenna. Consequently, the relative weights of the RGB components of each pixel are preserved and the image is transmitted without major losses. This experiment shows that our approach allows one to increase the information transfer rate to a given volume of space.

References and Notes

1. E. Betzig, J. K. Trautman, *Science* **257**, 189 (1992).
2. F. Zenhausern, Y. Martin, H. K. Wickramasinghe, *Science* **269**, 1083 (1995).
3. J. B. Pendry, *Phys. Rev. Lett.* **85**, 3966 (2000).
4. D. R. Smith, J. B. Pendry, M. C. K. Wiltshire, *Science* **305**, 788 (2004).
5. D. R. Smith, *Science* **308**, 502 (2005).
6. V. G. Veselago, *Sov. Phys. Usp.* **10**, 509 (1968).
7. N. A. Nicorovici, R. C. McPhedran, G. W. Milton, *Phys. Rev. B* **49**, 8479 (1994).
8. R. Shelby, D. R. Smith, S. Schultz, *Science* **292**, 77 (2001).
9. M. C. K. Wiltshire *et al.*, *Science* **291**, 849 (2001).
10. N. Fang, H. Lee, C. Sun, X. Zhang, *Science* **308**, 534 (2005).
11. D. O. S. Melville, R. J. Blaikie, *Opt. Exp.* **13**, 2127 (2005).
12. Z. Jacob, L. V. Alekseyev, E. Narimanov, *Opt. Exp.* **14**, 8247 (2006).
13. T. Taubner *et al.*, *Science* **313**, 1595 (2006).
14. M. Fink, *Phys. Today* **50**, 34 (1997).
15. C. Draeger, M. Fink, *Phys. Rev. Lett.* **79**, 407 (1997).
16. B. E. Henty, D. D. Stancil, *Phys. Rev. Lett.* **93**, 243904 (2004).
17. G. Lerosey, J. de Rosny, A. Tourin, A. Derode, M. Fink, *Phys. Rev. Lett.* **92**, 193904 (2004).
18. G. Lerosey, J. de Rosny, A. Tourin, A. Derode, M. Fink, *App. Phys. Lett.* **88**, 154101 (2006).
19. R. Carminati, J. J. Saenz, J.-J. Greffet, M. Nieto-Vesperinas, *Phys. Rev. A* **62**, 012712 (2000).
20. D. Cassereau, M. Fink, *IEEE Trans. Ultrason. Ferroelectr. Freq. Control* **39**, 579 (1992).
21. J. de Rosny, M. Fink, *Phys. Rev. Lett.* **89**, 124301 (2002).
22. Further details are available as supporting material on *Science* Online.
23. A. L. Moustakas, H. U. Baranger, L. Balents, A. M. Sengupta, S. H. Simon, *Science* **287**, 287 (2000).

24. This work was partially funded by the Agence Nationale de la Recherche under grant ANR-05-BLAN-0054-01.

Supporting Online Material

www.sciencemag.org/cgi/content/full/315/5815/1120/DC1
SOM Text
Fig. S1
References

7 September 2006; accepted 19 December 2006
10.1126/science.1134824

Downloaded from https://www.science.org at Indian Institute of Technology, Delhi on January 30, 2025

Redefining the Age of Clovis: Implications for the Peopling of the Americas

Michael R. Waters[1]* and Thomas W. Stafford Jr.[2]

The Clovis complex is considered to be the oldest unequivocal evidence of humans in the Americas, dating between 11,500 and 10,900 radiocarbon years before the present (^{14}C yr B.P.). Adjusted ^{14}C dates and a reevaluation of the existing Clovis date record revise the Clovis time range to 11,050 to 10,800 ^{14}C yr B.P. In as few as 200 calendar years, Clovis technology originated and spread throughout North America. The revised age range for Clovis overlaps non-Clovis sites in North and South America. This and other evidence imply that humans already lived in the Americas before Clovis.

For nearly 50 years, it has been generally thought that small bands of humans carrying a generalized Upper Paleolithic tool kit entered the Americas around 11,500 radiocarbon years before the present (^{14}C yr B.P.) and that these first immigrants traveled southward through the ice-free corridor separating the Laurentide and Cordilleran Ice Sheets (*1*). These people developed the distinctive lithic, bone, and ivory tools of Clovis (*2*, *3*) and then quickly populated

www.sciencemag.org/cgi/content/full/315/5815/1120/DC1

Supporting Online Material for

Focusing Beyond the Diffraction Limit with Far-Field Time Reversal

Geoffroy Lerosey, Julien de Rosny, Arnaud Tourin, Mathias Fink*

*To whom correspondence should be addressed. E-mail: mathias.fink@espci.fr

Published 23 February 2007, *Science* **315**, 1120 (2007)
DOI: 10.1126/science.1134824

This PDF file includes:

Supporting Online Material for

Focusing Beyond the Diffraction Limit with Far-Field Time Reversal

Geoffroy Lerosey, Julien de Rosny, Arnaud Tourin, Mathias Fink

Laboratoire Ondes et Acoustique, ESPCI, Université Paris VII, UMR 7587,

10 rue Vauquelin, 75005 Paris, France

This file includes :

SOM Text

Fig. S1

Supporting Online Material

1. The relation between the diffraction limit and the imaginary part of the Green's function

The origin of the diffraction limit, and the way to overcome it, can be completely revisited using the time-reversal concept. In any case (homogeneous or heterogeneous), the time-reversed wave which spatially converges to its source is immediately followed by a diverging wave due to energy flux conservation. Assuming a non-dissipative medium, a point-like source at $\mathbf{r_0}$ and a quasimonochromatic wavefield of angular frequency ω, the converging wave at point $\mathbf{r}$ is the advanced (or anticausal) Green function $G^-(\mathbf{r},\mathbf{r}_0;\omega)$ while the diverging wave is the retarded (or causal Green's function) multiplied by -1, i.e., $-G^+(\mathbf{r},\mathbf{r}_0;\omega)$ (the '-' comes from the π dephasing at the focusing point). The focusing spot is thus given by the imaginary part of the retarded Green's function (*S1*).

In the particular case of a purely homogeneous propagation medium, the converging wave at wavenumber k is given by $\frac{\exp(ik|\mathbf{r}-\mathbf{r}_0|)}{4\pi|\mathbf{r}-\mathbf{r}_0|}$, i.e., the advanced homogeneous Green's function between the source $\mathbf{r}_0$ and the observation point $\mathbf{r}$. As to the diverging wave, it is given by $\frac{\exp(-ik|\mathbf{r}-\mathbf{r}_0|)}{4\pi|\mathbf{r}-\mathbf{r}_0|}$, i.e., the retarded Green's function multiplied by –1. Finally it is the superposition of these two waves that produces the classical *sinc function* $\frac{\sin(k|\mathbf{r}-\mathbf{r}_0|)}{k|\mathbf{r}-\mathbf{r}_0|}$. As it has been shown, if an active source placed at the focusing point transmits a diverging wave opposite in phase with the one created by time-reversal, only the converging wave remains and the diffraction limit can be overcome (*S2*). This device acts as an acoustic sink that absorbs the TR wave. One severe drawback for applications is the need to use an active source at the focusing point to exactly cancel the usual diverging wave created during the focusing process.

As the focusing spot is also proportional to the imaginary part of the Green's function in the case of any heterogeneous non-dissipative medium, another more interesting and general approach consists in surrounding the focusing point by a microstructured medium with typical length scales well below the wavelength, e.g., putting some strong scatterers in the near-field of the source. In this case, the microstructured medium completely modifies the spatial dependence of the imaginary part of the Green's function that now oscillates on scales smaller than the wavelength. This is exactly the idea we exploit to create focal spots much smaller than the wavelength.

2. Description of the electromagnetic time-reversal mirror (TRM)

The experimental setup for time reversal of electromagnetic waves is depicted in Fig. S1. It is controlled by a central computer. On the transmit side, a two-channel generator (Tektronix AWG520) feeds a wideband 150-MHz bandwidth IQ modulator (RFMD2480) to produce an electromagnetic pulse centered at 2.45 GHz. As to the receive side, a very high bandwidth scope (Tektronix TDS6604), with a sampling rate of 20 GS/s, is used to record directly the RF signal. In addition, a pair of eight-channel switches is used, one to emulate an eight-channel TRM, the other one to emulate a eight-channel receiver.

The time-reversal operation consists in three steps:

- First, a 10-ns long 2.45 GHz RF pulse $e(t)$ is synthesised thanks to the IQ modulator feeded by the 2-channel generator and sent by antenna *#j* of the micro-structured array and the field $h(r_j,r_i\ ;t)$ is recorded at antenna *#i* of the TRM.
- In the second step, the signals $h(r_j,r_i\ ;t)$ are flipped in time. The I and Q components of $h(r_j,r_i\ ;t)$ are extracted numerically using a standard demodulation technique.
- In a third step, after a down conversion from 20 GS/s to 1 GS/s (i.e, the 2-channel generator sampling rate), the I and Q signals are loaded into the 2- channel generator of which the outputs are used to modulate the carrier at 2.45 GHz. The resulting signal is

sent back by antenna *#i*. Using the switch, the signals are successively received at the eight antennas of the receiving array and stored in the computer.

An equivalent way (used in our experiment) to perform the first step is to record the response $h(r_i,r_j\ ;t)$ at antenna *#j* of the micro-structured array when the pulse $e(t)$ is sent from antenna *#i* of the TRM. Thanks to the reciprocity theorem, $h(r_i,r_j\ ;t)= h(r_j,r_i\ ;t)$. Doing this way is advantageous because only one RF-generator (for the TRM) and one RF-receiver (for the microstructured array) are needed.

To emulate a *N*-channel TRM, this operation is repeated for the *N* antennas of the transmitting array and the corresponding signals received at each antenna of the receving array are summed to produce the signal that would be produced by a *N*-channel TRM.

In practise, two normalisations are actually performed: one after the signals have been flipped in time (step 1 of the time-reversal process), the other after reception at the microstructured array (step 3 of the time-reversal process). This procedure is needed to compensate for the differences in the sensitiviy of the microstrutured antennas forming the receiving array as explained in the next part.

3. Sensitivity compensation between antennas in the microstructured antenna array

The antennas of the microstructured array exhibit strong sensitivity fluctuations. There are at least two reasons for that. First, there may be a slight mismatch between the antenna heights. Second, the radiation mechanism of these antennas is sensitive to the positions of the copper wires around them. Indeed, the radiation is mainly due to conversion of evanescent components into propagative ones. Consequently, the field transmitted by one antenna is very dependent on its distance from the wire scatterers around it.

To correct for these sensitivity fluctuations, we apply a compensation factor for each antenna of the microstructured array. To that goal, before the time-reversal experiment itself, all the responses $h(r_i,r_j;t)$ are recorded. Then the factor α_j for antenna #j is calculated as:

$$\alpha_j = \sqrt{\sum_{i=1}^{N} \int h^2(r_i,r_j;t)dt} \ .$$

During the first step of the time-reversal process, the sensitivity mismatch on the transmit side is compensated for by sending $e(t)/\alpha_j$ instead of $e(t)$ by antenna #j of the sub-wavelength array.

During the third step of the time-reversal process, the signals recorded at each antenna #j of the microstructured array are divided by α_j to compensate for the sensitivity mismatch on receive side.

Thanks to this normalisation procedure, the refocused pulses have an amplitude about unity (Fig. 2).

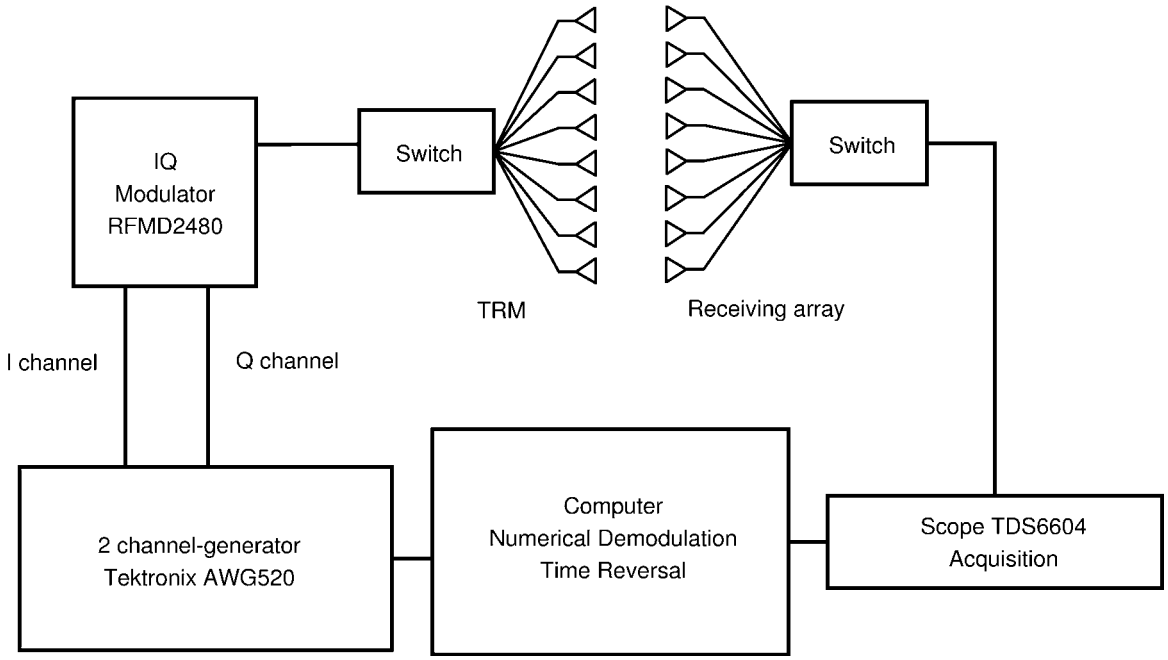

Fig. S1: Schematic diagram of the time-reversal system

References

S1. D. Cassereau and M. Fink, IEEE Trans. Ultrason. Ferroelectr. Freq. Control **39**, 579 (1992)

S2. J. de Rosny and M. Fink, Phys. Rev. Lett. **89**, 124301 (2002)